

See discussions, stats, and author profiles for this publication at: <https://www.researchgate.net/publication/339978831>

Design Validation and Performance Evaluation of a BLDC of Commercial Electric Bike and Its Performance Comparision with Different Probable Designs

Conference Paper · December 2019

DOI: 10.1109/NPEC47332.2019.9034747

CITATIONS

0

READS

61

3 authors:



Aditya Raj

Indian Institute of Engineering Science and Technology, Shibpur

1 PUBLICATION 0 CITATIONS

[SEE PROFILE](#)



Sourabh Paitandi

Indian Institute of Engineering Science and Technology, Shibpur

9 PUBLICATIONS 14 CITATIONS

[SEE PROFILE](#)



Mainak Sengupta

Indian Institute of Engineering Science and Technology, Shibpur

69 PUBLICATIONS 178 CITATIONS

[SEE PROFILE](#)

Some of the authors of this publication are also working on these related projects:



Switched reluctance motors and their converters for traction motors, pump applications and direct wheel drives [View project](#)



Induction heating Converters [View project](#)

Design Validation and Performance Evaluation of a BLDC of Commercial Electric Bike and Its Performance Comparision with Different Probable Designs

¹Aditya Raj, ²Sourabh Paitandi, and ³Mainak Sengupta

Dept. of Electrical Engineering

Indian Institute of Engineering Science and Technology, Shibpur, Howrah, W.B., India

Email: ¹adityaraj.dd2015@ee.iests.ac.in, ²sourabh350@gmail.com, ³msg@ee.iests.ac.in

Abstract—This paper presents the design validation and performance evaluation of a commercially available 8 pole, 12 slot, 3 phase, 1KW Interior Permanent Magnet (IPM) BLDC machine, used in popular commercial e-bikes. This machine has a fractional slot non-overlapping (concentrated) winding. The slots per pole per phase (SPP) is 0.5. The intricate design details of the machine have been extracted otherwise and validated analytically. With the extracted dimensional details (not available in datasheets), the machine has also been simulated in 2D-FEM and the parameters and performance indices have been duly calculated. Different performance indices such as THD in induced emf, iron and magnet losses, cogging torque, etc. have also been investigated in detail. The performance of the above mentioned machine has been compared against designs with other possible slot-pole combinations with SPP=0.25 and 0.375, but of same nominal ratings. Appropriate inferences and conclusions are thereby drawn.

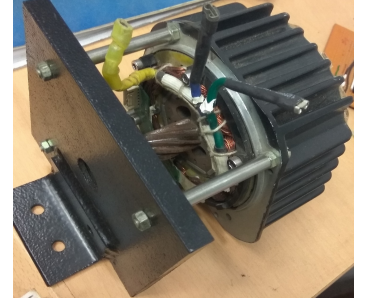
Index Terms—Brush-less, IPM, Non-overlapping concentrated winding, Finite element method, d and q-axis inductance

I. INTRODUCTION

The permanent magnet electrical machines are gaining attention due to their reduced losses and compact size that gives them a decisive edge for use in automotive applications. For a given power output, the PM machines have higher energy efficiency, lesser volume, higher power factor and easier controllability, than other rotating machines [1] [2]. Research on these machines also aims to develop them to be produced at an affordable price. This can help to reduce the carbon footprints of the country on a large scale. Brushless DC machine is such a machine and is well known in these applications due to its high efficiency, high reliability, long lifetime, simple design, low noise and good torque-speed characteristics [3] [4]. With the technological boon in power electronics, control and automation, speed regulation techniques of such machines are being improved for better performance and lesser cost [3] [6] [7] [8]. Non-overlapping windings are now being used for these machines, instead of the conventional distributed double layer windings chiefly, due to cost savings and simpler manufacturing process [5] [10] [11]. These have fractional slots per pole per phase (SPP), which lowers the alignment between the stator teeth and the magnet poles, and hence lowers the cogging torque too [12]. Additionally, due to shorter end-windings, these windings are compact [5], and have lower stator copper losses [12] and lower end-winding copper consumption [5]. This also allows for a lesser active length [13]. These machines also consume a lower lamination material due to lower stator yoke depth. However, the



(a) BLDC motor fitted with its controller and ebike pedal



(b) BLDC motor detached from ebike setup with an arrangement of free run

Fig. 1: The BLDC motor investigated

presence of lower order harmonics in the air gap flux distribution is more, causing higher losses in the rotor magnets and back-iron [12]. Hence, the PM machines have to be designed with minimum iron losses. For this, the best choices for number of poles are four, six and eight [1], particularly when the rated speed is higher. Now, BLDC machines with such concentrated winding have a range of SPP from 0.25 to 0.5.

This work was triggered when the authors were approached by a US-based popular manufacturer of electric bicycles. The IPM BLDC machine investigated here in this paper is the one that is commercially used in those electric bicycles, and is shown in Fig.1(b).

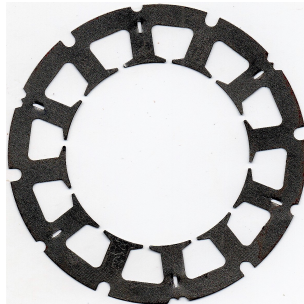
The BLDC studied here has non-overlapping concentrated winding with an SPP= 0.5 (3 phase, 8 pole,12 slot). The performance and parameters of such concentrated winding machines majorly depends on the slot-pole combinations of the machine [14]. Hence this has to be selected appropriately. Since the SPP is less than unity, the space available for slots is sufficient [9]. This paper deals with the detailed investigation and parameter estimation of the 3 phase, 8 pole, 12 slot BLDC machine. Two other BLDC designs with same nominal ratings and main dimensions with different slot numbers have been studied to investigate the effect of slot-pole combinations on performance of such machines.

II. DIMENSIONAL DETAILS OF THE BLDC MACHINE

As already mentioned, the machine was provided by a US-based seller of electric bicycles and the motor did not have any available datasheet or design sheet. Also it was so compact that nothing



(a) Image of the stator of dismantled machine with one turn of a phase dewound



(b) Stator stamping of the BLDC machine

Fig. 2: Images of the BLDC machine under rewinding

could be measured. Hence it had to be completely dismantled and rewound (to get the dimensions, winding details and even the SWG of the conductors) at the works of a small local manufacturer of electric machines. A photo of the dismantled machine stator is shown in Fig.2(a), and one stator stamping has been highlighted in Fig.2(b). The complete specifications of the BLDC machine, obtained after its re-winding, are listed in Table-I . Many of these values had to be tediously measured from the dismantled machine.

TABLE I: General details of the BLDC machine

Parameter name	Value
Rated shaft output power (in KW)	1
Rated armature current (in A)	30
Rated frequency (in Hz)	200
Rated speed (in rpm)	3000
Rated torque (in Nm)	3.183
Inbuilt controller rating	48V DC-link, 30A
Type of machine	Inner rotor IPM BLDC
Number of pole pairs	4
Number of slots	12
Slots per pole per phase (SPP)	0.5
Winding type	Fractional slot whole-coiled concentrated winding
Coils per phase	4
Turns per coil	9
Conductor specifications	10 strands of SWG 25 wires (Bare diameter=0.5mm and insulation thickness=35 μ m)
Stator outer diameter (in mm)	97.8
Stator inner diameter (in mm)	60
Stator stacking factor	0.95
Rotor stacking factor	0.95
Rotor outer diameter (in mm)	58.18
Rotor inner diameter (in mm)	12.8
Stator core material	M1924G
Rotor core material	M1924G
Skew width (in no. of slots)	0
Bearing type	628RS
Stator active length (in mm)	48.1
Rotor active length (in mm)	47.14

The 2D-FEM simulation of the machine has been done using these details. The associated parameters like slot fill factor and pole embrace have been calculated for simulation purposes, and come out to be 36.54% and 0.81 respectively.

III. DESIGN VALIDATION

The following features of the motor were practically observed and are theoretically validated:

A. Winding layout

The theoretical winding layout for an 8 pole 12 slot star connected concentrated winding machine is determined using the Cros' method [16]. For sake of continuity, it has been repeated here for the chosen 8 pole 12 slot BLDC:-

- 1) The number of slots per pole per phase, i.e., SPP, can be written as :

$$SPP = \frac{12}{3 * 8} = \frac{1}{2} = \frac{N}{D} \quad (1)$$

- 2) A sequence of zeros and ones is determined from (1) [16]. For this combination, N = 1 one and D-N = 1 zero. The first sequence is 10.
- 3) According to Cros' [16], the highest winding factor can be achieved when the sequence is as regular as possible. The most regular combination for this case also happens to be 10.
- 4) This regular sequence is repeated for, $\frac{N_s}{N} = \frac{12}{1} = 12$ times. Hence, the final sequence is:

$$\underbrace{10|10|10|...|10}_{12 \text{ times}}$$

- 5) Above sequence is compared to the layout of the distributed winding with SPP = 1.

$$\begin{array}{ccccccccccccc} 10 & 10 & 10 & 10 & 10 & 10 & 10 & ... \\ AC' & BA' & CB' & AC' & BA' & CB' & ... \end{array}$$

where A', B', C' are the return conductors of A, B, C

- 6) The start-phases of each-slot are follows:

$$\begin{array}{ccccccccccccc} \text{Phase : } A & & B & & C & & A & & B & & C \\ \text{Slot : } 1 & & 2 & & 3 & & 4 & & 5 & & 6 \end{array}$$

All the steps mentioned above are concisely presented in Fig. 4, where $S_x(x = A, B, C)$ are the slot vectors involved with the corresponding phase and slot number for a double layer winding. The resulting winding pattern, as shown in Fig.3, completely agreed with that observed upon re-winding.

B. Analytical calculation of induced emf

The winding configuration, as validated, and the other dimensions, as discussed earlier, have been used to simulate the machine in 2D-FEM. The flux density plots are obtained at a particular rotor position (as shown in Fig.-5 and Fig.-6). This is used for theoretical calculation of the fundamental component of the line induced emf using the Faraday's law, following,

$$\begin{aligned} e_{an} &= -\frac{d\psi_p}{dt} \\ \psi_p &= T_p * \phi = T_p * B_m * A_t * \sin(\omega * t) \end{aligned} \quad (2)$$

$$\text{or, } e_{ab} = \sqrt{3} * T_p * B_m * W_t * L * \omega * \sin(\omega * t - \frac{\pi}{3})$$

where, $\psi_p \triangleq$ flux linkage per phase; $e_{ab} \triangleq$ line induced emf; $T_p \triangleq$ turns/phase; $B_m \triangleq$ maximum magnetic flux density through phase turn (i.e., through a stator teeth); $W_t \triangleq$ tooth or phase turn width; $L \triangleq$ stator active length; $\omega \triangleq$ electrical angular frequency.

The value obtained using (2) has been compared with the emf plots directly obtained from 2D-FEM (shown in Fig.7), and, with the emf waveform obtained experimentally from the BLDC machine (shown in Fig.8). The comparisons are listed in Table- II.

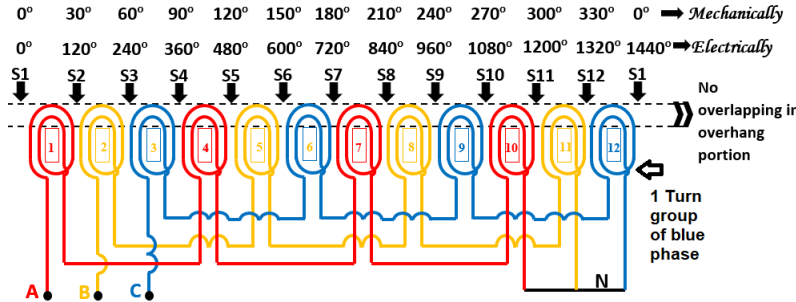


Fig. 3: Winding layout of 8 pole 12 slot 3 phase (SPP $q = 0.5$) IPM - BLDC motor

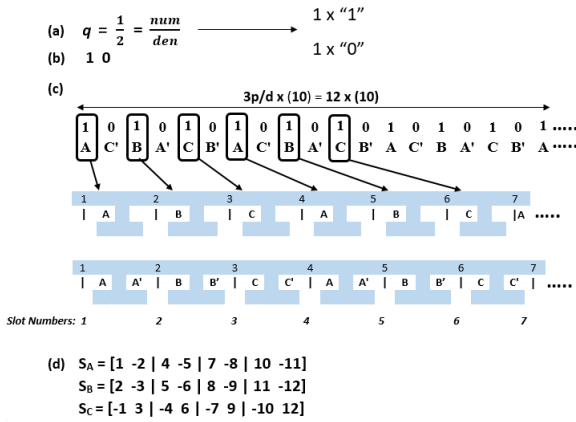


Fig. 4: Steps for Cros' method to determine winding layout [16]

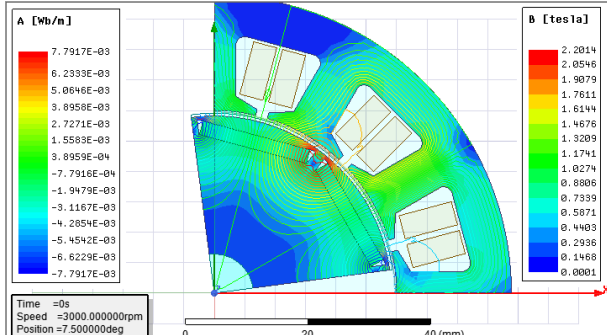


Fig. 5: 2D-FEM Analysis: Flux density map for the BLDC machine at 7.5°_{mech}

C. Relation between peak values of trapezoidal emf and its fundamental component

The fundamental peak is given by (3)

$$\hat{e}_{ab} = \frac{\sqrt{3}}{\pi} \int_0^{2\pi} e_{pt} \sin \theta d\theta \quad (3)$$

From the odd symmetry, (3) reduces to (4)

$$\hat{e}_{ab} = \frac{2\sqrt{3}}{\pi} \int_0^{\pi} |e_{pt}| \sin \theta d\theta \quad (4)$$

Putting the expression for e_{pt} , we get (5)

$$\begin{aligned} \hat{e}_{ab} = \frac{2\sqrt{3}}{\pi} & \left[\int_0^{\pi/6} \frac{6 * E_{ptm} * \theta}{\pi} * \sin \theta d\theta + E_{ptm} * \int_{\pi/6}^{5\pi/6} \sin \theta d\theta \right. \\ & \left. + \int_{5\pi/6}^{\pi} \frac{6 * E_{ptm} * (\pi - \theta)}{\pi} * \sin \theta d\theta \right] \end{aligned} \quad (5)$$



Fig. 6: 2D-FEM Analysis: Air gap flux density map for the BLDC machine at 7.5°_{mech}

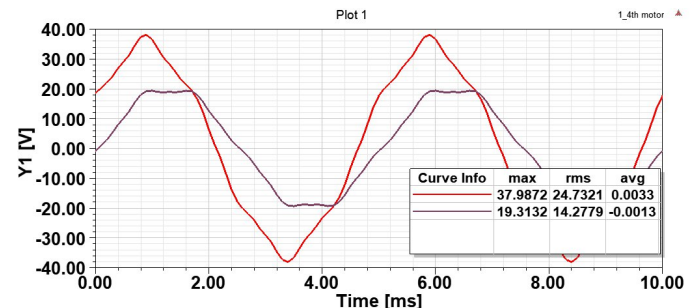


Fig. 7: 2D FEM Analysis Line and phase induced emf

(5) on simplification, leads to (6)

$$\hat{e}_{ab} = 2.1059 E_{ptm} \quad (6)$$

From the calculated value shown in Table II and (6), $E_{ptm} = \frac{36.3}{2.1059} = 17.237$ V

D. Conductor dimensions

From (7) [17], the rated DC-link current= 29 A and rated phase current = 23.7 A. Rotor losses have been neglected here. Assuming a current density of 12 A/mm^2 , the bare diameter of each conductor strand=0.5 mm (SWG-25). The values matched under tolerable limits from practical observations during re-winding.

$$P_{air\ gap} \approx P_{shaft} = 2 * E_{ptm} * I_{dc} \quad (7)$$

$$I_{ph} = \sqrt{\frac{2}{3}} * I_{dc}$$

where E_{ptm} - peak value of phase induced emf

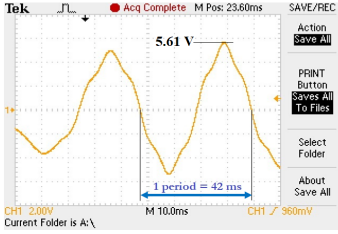


Fig. 8: Line induced emf from manual run as generator at 357 rpm, ($r_{ms} = 3.38V$), ($\text{Avg.} = 0.006137V$)

TABLE II: Comparision of line induced emf(s) from FEM and practical

Parameter	From FEM simulation	From theoretical calculation	From manual run
Speed of run (in rpm)	3000	3000	357
Electrical frequency (in Hz)	200	200	23.8
RMS value (in V)	24.73	25.67	3.73
Peak value (in V)	38	36.30	5.61
RMS/electrical frequency (in Vs)	0.124	0.128	0.157

IV. PARAMETER EXTRACTION

The important parameters such as needed for the mathematical modelling have been calculated theoretically and validated through 2D FEM simulation and practical experiment.

A. Phase Resistance

The phase resistance is theoretically calculated using (8).

$$R = \rho_{Cu} \times \frac{L_{mts}}{A} = \rho_{Cu} \times \frac{(2L + \pi\tau_s)}{A} \quad (8)$$

where the symbols have their conventional meanings. The value obtained has been matched against the values obtained from the FEM simulation in Table- III.

TABLE III: Comparision of values of resistances (in Ω) obtained through various means

From theoretical calculation	From 2D FEM simulation	From practical determination
0.05	0.05	0.047

B. Inductances at no-load

The profile of phase self inductance and inter-phase mutual inductance under no-load, as a function of the position of the salient rotor is obtained using 2D-FEM simulation and shown in Fig.-9.

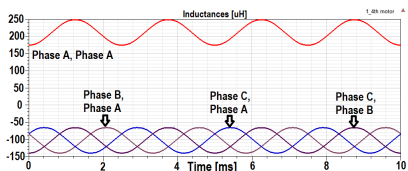
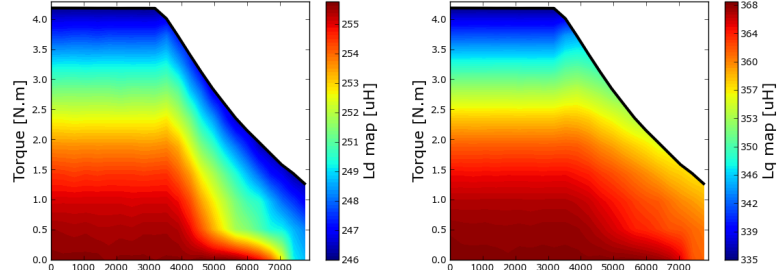


Fig. 9: 2D FEM Analysis: Inductance waveforms at no load for the BLDC Machine



(a) L_d contour

(b) L_q contour

Fig. 10: 2D FEM simulation: Torque-speed map with inductance contours

C. d and q axis inductances (L_d , L_q)

The L_d and L_q of the machine at different operating conditions of torque and speed have been obtained from its 2D-FEM simulation and are shown in Fig.10(a) and Fig.10(b) respectively. The inductances are seen to remain constant upto the rated speed for a given torque output, and they tend to decrease at speeds higher than rated (in the flux weakening zone). Hence the currents will follow a reverse pattern, i.e., constant at a low value upto rated speed and reduce thereafter. At a given speed, the inductances decrease and hence allow the currents to increase and hence to increase the torque output.

The values of the inductances at rated speed and torque have been analytically validated as follows:-

The self and mutual inductances of a synchronous machine can be written as [18],

$$\begin{bmatrix} L_{aa} \\ L_{ab} \\ L_{ac} \end{bmatrix} = \begin{bmatrix} 1 & 1 & \cos 2\theta_r \\ 0 & -\frac{1}{2} & \cos 2(\theta_r - 120^\circ) \\ 0 & -\frac{1}{2} & \cos 2(\theta_r + 120^\circ) \end{bmatrix} \begin{bmatrix} L_l \\ L_1 \\ L_2 \end{bmatrix} \quad (9)$$

The d and q axis inductances are given by [18],

$$\begin{bmatrix} L_d \\ L_q \end{bmatrix} = \begin{bmatrix} 1 & \frac{3}{2} \\ 1 & -\frac{3}{2} \end{bmatrix} \begin{bmatrix} L_l \\ L_1 \\ L_2 \end{bmatrix} \quad (10)$$

From (10), L_2 is negative for this machine because here $L_q > L_d$. Hence, the following equations are derived (using Fig.9),

$$\begin{bmatrix} L_{aa,max} \\ L_{aa,min} \\ L_{ab,max} \\ L_{ab,min} \\ L_{ac,max} \\ L_{ac,min} \end{bmatrix} = \begin{bmatrix} 1 & 1 & -1 \\ 1 & 1 & 1 \\ 0 & -\frac{1}{2} & -1 \\ 0 & -\frac{1}{2} & 1 \\ 0 & -\frac{1}{2} & -1 \\ 0 & -\frac{1}{2} & 1 \end{bmatrix} \begin{bmatrix} L_l \\ L_1 \\ L_2 \end{bmatrix} = \begin{bmatrix} 248.3855 \\ 174.3666 \\ -65.6856 \\ -139.9572 \\ -65.6673 \\ -139.9564 \end{bmatrix} \quad (11)$$

The units on RHS of the equations are in μH . Hence, $L_1 = 205.6428 \mu\text{H}$, $L_l = 5.73325 \mu\text{H}$ and $L_2 = -37.1358 \mu\text{H}$. The values hence obtained for L_d and L_q have been compared with those obtained from Fig.10(a) and Fig.10(b) respectively, in Table IV

TABLE IV: Comparision of d and q axis inductances at rated speed and torque for the IPM BLDC machine

Parameter	Approx. value from contour map (μH)	Value from analytical calculation(μH)
L_d	251	258.5
L_q	350	369.9

V. PERFORMANCE EVALUATION

The efficiency of the machine has been investigated at different operating conditions of torque and speed using the 2D-FEM simulation and is presented in Fig.11. At a given torque output, the efficiency is seen to increase upto rated speed and thereafter decrease in the flux weakening zone. A similar pattern is seen for efficiency at a given speed with varying torque output. The efficiency is seen to be maximum in a zone where speed is near the rated and output torque is lesser than rated.

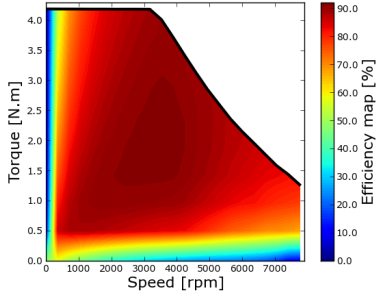


Fig. 11: 2D-FEM simulation: Efficiency map for the IPM BLDC machine

The efficiency is analytically validated for the rated condition. Analytical validation is done using the loss data at rated speed obtained from the 2D-FEM simulation, tabulated in Table V. Rated efficiency = $\frac{1000}{1160.44} = 86.17\%$ (From Fig.11, it is $\approx 87\%$), which is very high for such a small motor.

TABLE V: Components of core losses of the BLDC machine

Loss component	Average value for stator (in W)	Average value for rotor (in W)	Total average value (in W)
Hysteresis loss	4.884	0.0242	4.9082
Eddy current loss	9.5218	0.1315	9.6533
Excess loss	0.769	0.016	0.785
Total core loss	15.2378	0.1739	15.4117
Magnet loss	N.A.	0.034	0.034
Copper loss (at rated current)	135	N.A.	135
Friction and windage loss (assumed 1% of rated output)	N.A.	N.A.	10
Total losses	150.2378	0.2079	160.4457

The practical estimation of efficiency is under progress and the rewound motor is coupled with a brake-pulley loading arrangement and an optical position sensor to run it in 120° conduction mode using the fabricated logic circuit. The setup operation with waveforms of line voltage (V_{RY}) and current (I_R) is shown in Fig.12. It must be mentioned that the integrated motor plus power converter and controller were all otherwise in a working condition in a nicely compact but inaccessible contraption connected with pedals.

VI. COMPARISON OF THE BLDC MACHINE WITH OTHER SLOT-POLE CONFIGURATIONS

The performance indices of BLDC designs having different SPPs (same no. of poles but different slot count) but similar voltage and torque ratings have been compared and tabulated in Table VI. The induced emf per phase at rated speed for the three design variants have been obtained from their 2D-FEM simulation and are compared in Fig.13. The *rms* values of different odd harmonic components in the induced emf per phase have been shown in Fig.14

TABLE VI: Comparision of parameters in different slot-pole configurations

Parameters	12 slot/8pole	9 slot/8pole	6 slot/8pole
Turns per phase coil	9	11	17
SPP	0.5	0.375	0.25
Winding factor	0.866	0.945	0.866
THD in induced emf per phase (%)	6.74	11.47	5.12
C_T [15]	4	1	2
Torque ripple factor	0.181	0.058	0.224
Torque density (Nm/kg)	1.813	1.845	1.812
Core loss at full load (W)	24.6	24.5	27.5
Magnet loss (W)	0.9	5.35	20.54
L_d (μ H)	223.8	253.2	520.7
L_q (μ H)	334.2	361.9	615

for each of the design variants. The 9 slot design (SPP=0.375) is seen to be rich in third harmonics and has the worst THD among all the chosen designs, though it has lower losses and lower cogging torque, that adds to lowest torque ripple among the considered designs. The other two designs have lower triplen harmonics, and have a better THD. The 6-slot design (SPP =0.25) has the best THD but suffers from greater losses and cogging leading to more torque ripple.

The cogging torque for the three design variants have been obtained from their 2D-FEM simulation and are compared in Fig.15. The 8 pole 9 slot variant has the lowest cogging torque (40 mNm), and the 8 pole 6 slot has the maximum value (520 mNm). The relative estimator for cogging torque as mentioned in [15] is seen to hold good for 9 slot design, as it has the lowest C_T among all designs. But for the other two design variants, the one with a higher C_T is seen to have slightly lower cogging torque. This needs an in-depth validation.

VII. CONCLUSIONS

The winding layout of the machine as proposed using Cros' method matched with the practical observation of the armature upon its de-winding. The calculated back emf constant and conductor dimensions were close to the practical observations under tolerable limits. L_d and L_q calculated using self and mutual inductance values from FEM have a very good match with those directly given by FEM maps. The motor loading tests are in progress to validate the proposed performance indices obtained from FEA. The mentioned design validations have been done upon specific approach by the sellers of the commercial ebikes.

On comparing the said machine with some other possible design variants with nominal ratings, it has satisfactory performance indices, intermediate of the other two designs and hence appears to be a better design to be implemented in a hardware prototype for the mentioned ratings.

VIII. ACKNOWLEDGEMENTS

The authors extend their special thanks to D. Snyder of California, USA, the staff of M/S GE motors Pvt. Ltd, Sheorapuli, and Mr. S K Mainuddin for their notable help in the entire process. The support received from the research colleagues, staff, particularly Mr. Netai Dutta, at the Advanced Power Electronics Lab, and the authorities of IEST, Shibpur is also gratefully acknowledged.

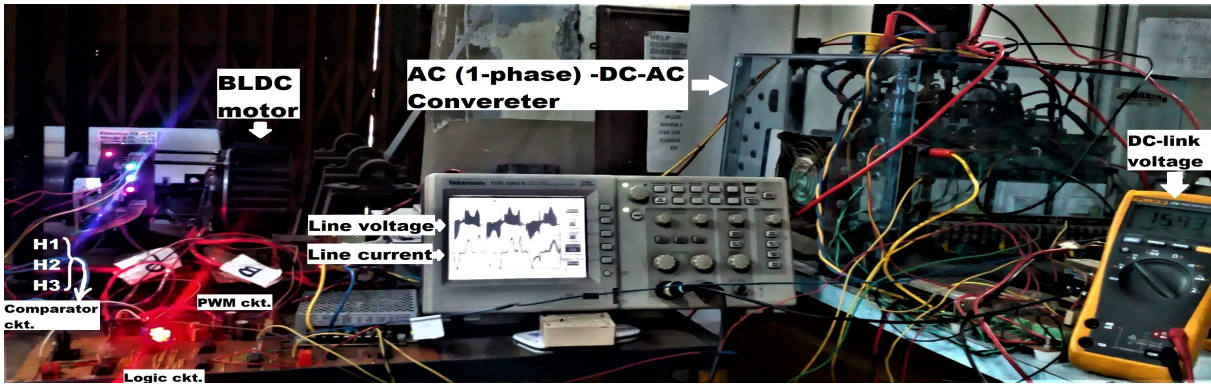


Fig. 12: Practical setup for efficiency estimation

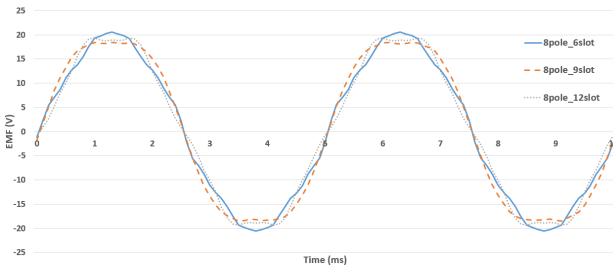


Fig. 13: 2D-FEM simulation: Induced emf at rated speed

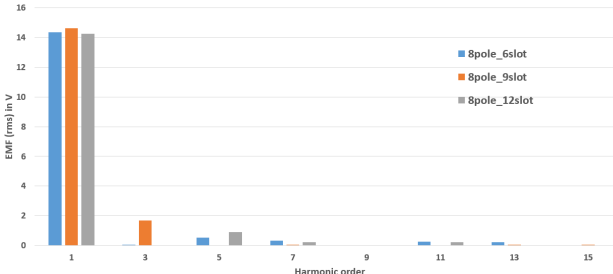


Fig. 14: Odd harmonic spectrum of induced emf(s)

REFERENCES

- [1] Chunting Chris Mi, Senior Member, IEEE, Gordon R. Slemon, Life Fellow, IEEE, and Richard Bonert, Member, IEEE, "Minimization of Iron Losses of Permanent Magnet Synchronous Machines.", *IEEE Transactions on Energy Conversion*, vol. 20 , issue. 1 , Mar, 2005, DOI:10.1109/TEC.2004.832091
- [2] Anqing He, Chenxi Zhou, et.al. "Evaluation of Fractional Slot Concentrated Winding Permanent Magnet Synchronous Machine for Electric Vehicle Application", *IEEE International Electric Machines & Drives Conference (IEMDC)*, May, 2019, DOI: 10.1109/IEMDC.2019.8785223
- [3] Chang-liang Xia, Tianjin University, P.R. China, "PERMANENT MAGNET BRUSHLESS DC MOTOR DRIVES AND CONTROLS", ISBN:9781118188330
- [4] Y.B. Adyapaka Apatya, Aries Subiantoro and Feri Yusivar, "Design and Prototyping of 3-Phase BLDC Motor", *International Conference on Quality in Research (QIR) : International Symposium on Electrical and Computer Engineering*, July, 2017, DOI:10.1109/QIR.2017.8168483
- [5] Dieter Gerling,"Electrical Machines Mathematical Fundamentals of Machine Topologies",pp-449, ISBN:9783662520321
- [6] Józef Gromba, "Torque Control of BLDC Motor for Electric Bicycle", *International Symposium on Electrical Machines (SME)*, June 2018, DOI:10.1109/ISEM.2018.8442987
- [7] Vladimir Dimitrov, "Overview of the Ways to Design an Electric Bicycle", *National Conference with International Participation (ELECTRONICA)*, May, 2018, DOI:10.1109/ELECTRONICA.2018.8439456
- [8] K. Latha Shenoy, M. Satyendra Kumar, "Design Topology and Electromagnetic Field Analysis of Permanent Magnet Brushless DC Motor for Electric Scooter Application", *International Conference on Electrical, Electronics, and Optimization Techniques (ICEEOT)*, March 2016, DOI:10.1109/ICEEOT.2016.7754942
- [9] Florence Meier, "Permanent-Magnet Synchronous Machines with Non-Overlapping Concentrated Windings for Low-Speed Direct-Drive Applications"
- [10] T. D. Strous, H. Polinder, Member, IEEE, J. A. Ferreira, Fellow, IEEE,"Inductance calculations for PM machines with concentrated windings", *IEEE International Electric Machines & Drives Conference (IEMDC)*, May, 2011, DOI:10.1109/IEMDC.2011.5994636
- [11] Freddy Magnusson, Member, IEEE, and Heinz Lendenmann, Member, IEEE, "Parasitic Effects in PM Machines With Concentrated Windings", *IEEE TRANSACTIONS ON INDUSTRY APPLICATIONS*, VOL. 43, NO. 5, SEPTEMBER/OCTOBER 2007, DOI:10.1109/TIA.2007.904400
- [12] Chun Tang, Wen L. Soong, Gene S. Liew and Nesimi Ertugrul, "Effect of Pole and Slot Number Changes on the Performance of a Surface PM Machine", *International Conference on Electrical Machines*, Sep, 2012, DOI:10.1109/ICELMach.2012.6349867
- [13] Design and Optimization of Interior PM Machines with Distributed and Fractional-Slot Concentrated- Windings for Hybrid Electric Vehicles, *IEEE Conference and Expo Transportation Electrification Asia-Pacific (ITEC Asia-Pacific)*, Sep, 2014, DOI:10.1109/ITEC-AP.2014.6941169
- [14] F. Libert, J. Soulard, "Investigation on Pole-Slot Combinations for Permanent-Magnet Machines with Concentrated Windings", Jan, 2004
- [15] Z.Q. Zhu and D. Howe, "Influence of Design Parameters on Cogging Torque in Permanent Magnet Machines," *IEEE Trans. Energy Conv.*, vol. 15, no. 4, pp. 407- 412, Dec. 2000., DOI:10.1109/60.900501
- [16] J. Cros and P. Viarouge, "Synthesis of high performance pm motors with concentrated windings", *IEEE Transactions on Energy Conversion*, vol. 17, no. 2, pp. 248-253, Jun. 2002
- [17] Bimal K. Bose, "Modern Power Electronics and AC Drives", ISBN: 9780130167439
- [18] D. O'Kelly and S. Simmons., Introduction to generalized electrical machine theory, 3d ed. McGraw-Hill European electrical engineering series, 1968, ISBN:9780070940505
- [19] Aditya Raj, B.Tech theses, "Investigations on Permanent Magnet Machines for Electric Vehicle Applications"

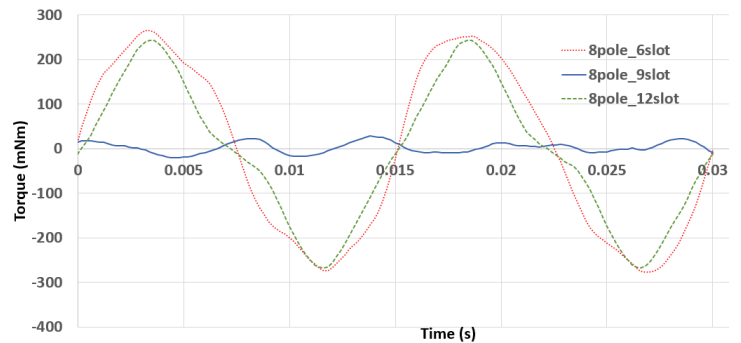


Fig. 15: 2D-FEM simulation: Cogging torques for the three BLDC designs